Adaptive Finite Element Computations of Shear Band Formation

Th. Baxevanis
Dept. of Applied Mathematics, Univ. of Crete, Heraklion 71409, Greece
theocharis@tem.uoc.gr

Th. Katsaounis
Dept. of Applied Mathematics, Univ. of Crete, Heraklion 71409, Greece
Institute of Applied and Computational Mathematics, FORTH, Heraklion 71110, Greece
thodoros@tem.uoc.gr

A.E. Tzavaras
Department of Mathematics, Univ. of Maryland, College Park, MD 20742, USA
Institute of Applied and Computational Mathematics, FORTH, Heraklion 71110, Greece
tzavaras@math.umd.edu

We study numerically an instability mechanism for the formation of shear bands at high strain-rate deformations of metals. We use a reformulation of the problem that exploits scaling properties of the model, in conjunction with adaptive finite element methods of any order in the spatial discretization and implicit Runge-Kutta methods with variable step in time. The numerical schemes are of implicit-explicit type and provide adequate resolution of shear bands up to full development. We find that already from the initial stages, shear band formation is associated with collapse of stress diffusion across the band and that process intensifies as the band fully forms. For fully developed bands, heat conduction plays an important role in the subsequent evolution by causing a delay or even stopping the development of the band.

Keywords: shear bands, localisation, adaptive finite elements

AMS Subject Classification: 22E46, 53C35, 57S20

1. Introduction

Shear bands are regions of intensely localised shear deformation that appear during the high strain-rate plastic deformation of metals. Once the band is fully formed, the two sides of the region are displaced relatively to each other, however the material still retains full physical continuity from one side to the other. Shear bands are often precursors to rupture and their study has attracted attention in the mechanics as well as the mathematics literature (see Refs. 35, 16, 39, 41 for surveys).

A mechanism for the shear band formation process is proposed in Ref. 15: Under isothermal conditions metals generally strain harden and exhibit a stable response. As the deformation speed increases, the heat produced by the plastic work triggers thermal effects. For certain metals, their thermal softening properties may outweigh

the tendency of metals to harden and deliver net softening response. This induces a destabilising mechanism, where nonuniformities in the strain-rate result in nonuniform heating, and in turn, since the material is harder in cold spots and softer in hot spots, the initial non-uniformity is further amplified. By itself this mechanism would tend to localise the total deformation into narrow regions. Opposed to this mechanism stands primarily the mechanism of momentum diffusion that tends to diffuse nonuniformities in the strain rate and second thermal diffusion that tends to equalise temperatures. The outcome of the competition depends mainly on the relative weights of thermal softening, strain hardening and strain-rate sensitivity, as well as the loading circumstances and the strength of thermal diffusion.

The following model, in non dimensional form, (described in detail in section 2) has served as a paradigm for the study of the instability mechanism

$$\begin{aligned} v_t &= \frac{1}{r}\sigma_x\,, \\ \theta_t &= \kappa\theta_{xx} + \sigma v_x\,, \\ \gamma_t &= v_x, \\ \sigma &= \theta^{-\alpha}\gamma^m\gamma_t^n\,, \end{aligned} \tag{1.1}$$

It models the balance of momentum and energy in simple shearing deformations of a thermoviscoplastic material with yield surface described by an empirical power law. The parameters $\alpha > 0$, $m > 0$ and $n > 0$ measure the degree of thermal softening, strain hardening and strain-rate sensitivity, respectively, while r and κ stand for dimensionless constants. The model (1.1) simulates the essential aspects of experiments like the pressure-shear test, see Ref. 16 or the thin-walled tube torsion test, see Refs. 26, 29. Moreover, shear bands typically appear and propagate (up to the interaction time) as one-dimensional structures, and a thorough understanding of the formation process is lacking even in that simple case. A number of investigations concerning (1.1) or variants thereof have appeared in the literature approaching the subject of shear band formation from a mechanics, see Refs. 15, 31, 32, 13, 11, analytical see Refs. 17, 37, 38, 39, 12, 7 or computational perspective, see Refs. 18, 42, 40, 21, 22, 4, 20, 36, 25, 19, 33, 8, 10. The reader is also referred to experimental, see Ref. 27, or computational studies, see Refs. 43, 13 of shear bands in several space dimensions.

A stability criterion was developed in Refs. 30, 31 using a linearized stability analysis of relative perturbations and some simplifying arguments. This analysis leads to the conclusion that (1.1) is stable when $q := -\alpha + m + n > 0$ and loses stability in the complementary region $q < 0$. This criterion corroborated well with non-linear stability results in Refs. 17, 37, 39 on various special cases as well as with non-linear criteria for instability, see Ref. 38 under prescribed stress boundary conditions. An effective equation describing the asymptotic in time response is derived in Ref. 28 and leads to a second order non-linear diffusion equation that changes type from forward to backward parabolic across the threshold $q = 0$. It is still an open question whether the solution, when $q = m + n - \alpha < 0$, blows up in

finite time or the solution exists for all times. Our numerical computations cannot provide a conclusive answer. Although the question is not relevant from a practical perspective, since real materials would fracture well ahead such a potential critical time, it is of mathematical interest and a computational challenge.

Our goal is to draw conclusions on the physics of the onset of shear band formation. In this work we perform a systematic numerical study of (1.1) based on

- an appropriate nondimensionalization followed by a change of time scale,
- special spatial and temporal adaptive techniques.

Many researchers gave numerical results that faithfully followed the process of localisation up to a point where resolution is lost as a result of insufficient mesh refinement. Wright and Walter, Refs. 42, 40 provide early computational studies of the evolution of an adiabatic shear band from the initial, nearly homogeneous stage to the fully localised stage. We refer to Refs. 4, 18, 22, 21, 20 for numerical computations of various one-dimensional models and to Refs. 2, 3 for two- and three-dimensional computational studies. In a different approach discontinuities of the displacement field (strong discontinuities) are embedded into the finite element spaces, see Refs. 36, 25, 19, 33, 8, 10.

In this work we use mesh adaptivity to resolve the shear band. We use continuous finite element spaces to approximate the unknown variables but their spatial derivatives are approximated by discontinuous elements. We propose special spatial and temporal refinement techniques to be able to capture correctly the multiscale nature of the shear band formation. The proposed adaptive mesh refinement techniques are motivated by works devoted to the resolution of blow-up problems, see Refs. 1, 9, 34 for semilinear parabolic or Schroedinger equations, in one or two space dimensions. These methods are well suited to handle shear bands and offer very good resolution up to full development. It should however be noted that the present computational context is more challenging as it involves resolution of a quasilinear hyperbolic-parabolic system. The spatial adaptation is based on a local inverse inequality satisfied by the finite element spaces in any space dimension, while the time step selection process is based on preserving an energy related to the system.

While adaptive techniques for computing shear band have been used by several authors the present methodology has certain novel features :

- detects in a automatic way the location of the shear band.
- it resolves the singularity by placing relatively few extra spatial grid points using an error estimator based on properties of the model.
- the mesh sizes around the singularity can be of order 10^{-13} of the size of the specimen, thus essentially overcoming the mesh dependency problem on resolving the shear band, while the discretization is coarser away from the singularity.
- due to the local nature of the spatial adaptive technique only one or two

elements are refined at each refinement step, thus the extra computational cost for computing the new finite element space as well as the related stiffness matrices, is rather small.
- it uses a physical property of the model as selection mechanism for the time step.

Regarding past work, we note the moving grid method developed in Ref. 18 to refine the mesh locally and reduce the discretization error, the local mesh refinement technique in Refs. 4, 5 that distributes uniformly over the domain certain scaled residuals of the solution, and the mesh refinement strategy of Ref. 20 based on *a-posteriori* error estimation. Finally, for computations of two-dimensional shear band models, the reader is referred to Ref. 6 (where the area of an element is taken inversely proportional to the value of the deformation measure at its centre) and to Ref. 24, where a combination of a front tracking method and error indicators are used to refine the mesh.

We perform computations first for the adiabatic model $\kappa = 0$ and then study the effects of heat conduction $\kappa > 0$. The effect of the heat diffusion on shear band formation was reported initially in Ref. 40, where based on numerical evidence, after a critical time the profile of the solution remain quasi-constant. Our results, for the adiabatic case, indicate strain localisation and shear band formation for parameter values in the region $q < 0$. It is shown that shear band formation is associated with a collapse of the stress-diffusion mechanisms across the cross-sectional location of the band (see Fig. 6) what is in accordance with the theoretical analysis in Ref. 28. Regarding the effect of heat diffusion, systematic computational runs indicate the following: heat diffusion does not affect much the time that localisation initiates, it affects considerably the rate of strain-rate growth inside the band, and it invariably delays and it can even stop the subsequent evolution of the localisation process. However, the stopping effect takes a long time to materialise, and in practical situations it could well be that the material will break before this effect is observed.

This paper is organised as follows: in Section 2 we introduce the mathematical model. The finite element approximations are described in Section 3 while in Section 4 several numerical results are presented.

2. Description of the model

From a mathematical perspective, shear band formation provides a fascinating example of competition between the non-linear instability mechanism induced by net softening response, with the stabilising effects of dissipative mechanisms (momentum and thermal diffusion). Its mathematical aspects are connected to resolving parabolic regularisations of ill-posed problems, see Ref. 39, what of course presents associated computational challenges. The mathematical model (2.1) is first nondimensionlized leading to the non-dimensional form (2.6). All material related characteristics are integrated in the two non-dimensional parameters, r and κ, in (2.6).

This system admits the special class of the uniform shearing solutions. We next introduce a reformulation of the problem, motivated by the form of the uniform shearing solutions and a time rescaling of exponential type, see (2.14). The resulting re-scaled system (2.15) captures the scaling characteristics of the problem. Its use allows to achieve very long times in the numerical computations with considerably smaller computational effort, and enables us to draw conclusions on the physics of the onset of localisation and reveal physical features of the model in particular in the non-adiabatic case.

As shear bands appear and propagate as one-dimensional structures (up to interaction times) most investigations have focused on one-dimensional, simple shearing deformations. An infinite plate located between the planes $x = 0$ and $x = d$ is undergoing a simple shearing motion with the upper plate subjected to a prescribed constant velocity V and the lower plate held fixed. The equations describing the simple shear,

$$\begin{aligned} \rho v_t &= \sigma_x \,, \\ \gamma_t &= v_x \,, \\ c\rho\theta_t &= k\theta_{xx} + \sigma\gamma_t \,, \end{aligned} \tag{2.1}$$

describe the balance of momentum, kinematic compatibility and balance of energy equations, the quantities appearing in them are the velocity in the shearing direction $v(x,t)$, plastic shear strain $\gamma(x,t)$, temperature $\theta(x,t)$, shear stress $\sigma(x,t)$, while the constants ρ, c, k standing respectively for the density, specific heat and thermal conductivity. Assumptions that have been factored in the model are that elastic effects as well as any effect of the normal stresses are neglected, that all the plastic work is converted to heat, and the heat flux is modelled through a Fourier law. The plates are assumed thermally insulated, that is $\theta_x(0,t) = \theta_x(d,t) = 0$.

For the shear stress we set

$$\sigma = f(\theta, \gamma, \gamma_t)\,, \tag{2.2}$$

where f is a smooth function with $f(\theta,\gamma,0) = 0$ and $f_p(\theta,\gamma,p) > 0$, for $p \neq 0$. The relation (2.2) may be viewed as describing the yield surface for a thermoviscoplastic material or (by inverting it) as a plastic flow rule, and we require that the material exhibits thermal softening, $f_\theta(\theta,\gamma,p) < 0$, and strain hardening $f_\gamma(\theta,\gamma,p) > 0$. The difficulty of performing high strain-rate experiments causes uncertainty as to the specific form of the constitutive relation (2.2). In the experimental and mechanics literature on high strain-rate plasticity, see Refs. 15, 16, 29, there is extensive use of empirical power laws,

$$\sigma = \mu_r \left(\frac{\theta}{\theta_r}\right)^{-\alpha} \left(\frac{\gamma}{\gamma_r}\right)^{m} \left(\frac{\gamma_t}{\dot\gamma_r}\right)^{n} = \mu\, \theta^{-\alpha}\gamma^m\gamma_t^n, \tag{2.3}$$

obtained by fitting experimental data to the form (2.3). The parameters $\theta_r, \gamma_r, \dot\gamma_r$ are the reference values of the temperature, strain and strain-rate associated to the determining experiment, while the material constant μ_r and the α, m, n are

obtained by fitting the data. The fitted values of α, m, n serve as measures of the degree of thermal softening, strain hardening and strain rate sensitivity for the material at hand. According to experimental data for most steels we have $\alpha = O(10^{-1})$, $m = O(10^{-2})$ and $n = O(10^{-2})$. In the case of the cold-rolled steel -AISI 1018, for example, with a constitutive law of the form (2.3), the following set of parameters are determined in Ref. 15:

$$\begin{aligned} &\mu = 436\ MPa, \quad \rho = 7800\ Kg/m^3, \quad c = 500\ J\ Kg^{-1}\ C^{-1}, \\ &k = 54\ W/(mC) \quad m = 0.015, \quad n = 0.019, \quad \alpha = 0.38. \end{aligned} \tag{2.4}$$

We refer to Refs. 15, 39, 41 for further details on the model, and to Ref. 29 for the experimental setup and an outline of how the data are fitted to power laws. The following nondimensionalization is also often employed:

$$\hat{x} = \frac{x}{d}, \qquad \hat{t} = t\dot{\gamma}_0, \qquad \hat{v} = \frac{v}{V}, \qquad \hat{\theta} = \frac{\theta}{\tau_0/\rho c}, \qquad \hat{\sigma} = \frac{\sigma}{\tau_0}, \tag{2.5}$$

where d is the specimen size, τ_0 stands for a reference stress to be appropriately selected, $\theta_0 = \frac{\tau_0}{\rho c}$ is a reference temperature and $\dot{\gamma}_0 = \frac{V}{d}$ is a reference strain rate. One then obtains the non-dimensional form

$$\begin{aligned} v_t &= \frac{1}{r}\sigma_x\,, \\ \theta_t &= \kappa\theta_{xx} + \sigma v_x\,, \\ \gamma_t &= v_x \end{aligned} \tag{2.6}$$

and

$$\sigma = \frac{1}{\tau_0} f\left(\frac{\tau_0}{\rho c}\theta, \gamma, \dot{\gamma}_0\gamma_t\right)\,,$$

for $(x,t) \in [0,1]\times[0,\infty)$ and where we dropped the hats. This system contains two non-dimensional numbers :

$$r = \frac{\rho V^2}{\tau_0}\,, \quad \kappa = \frac{k}{\rho c V d}, \tag{2.7}$$

where r is a ratio of stresses and depends on the choice of the normalising stress τ_0 and κ the usual thermal diffusivity. The reference stress τ_0 is useful in normalising the constitutive function f. For the empirical power law (2.3), by selecting $\tau_0 = \mu_r\left(\frac{\frac{\tau_0}{\rho c}}{\theta_r}\right)^{-\alpha}\left(\frac{1}{\gamma_r}\right)^m\left(\frac{\dot{\gamma}_0}{\dot{\gamma}_r}\right)^n$, we obtain the non-dimensional form

$$\sigma = \theta^{-\alpha}\gamma^m\gamma_t^n\,. \tag{2.8}$$

The parameters $\alpha > 0$, $m > 0$ and $n > 0$ serve as measures of the degree of thermal softening, strain hardening and strain-rate sensitivity. Another commonly used constitutive relation is the Arrhenius law

$$\sigma = e^{-\alpha\theta}\gamma_t^n\,. \tag{2.9}$$

In the form (2.9) the Arrhenius law does not exhibit any strain hardening and the parameters α and n measure the degree of thermal softening and strain-rate sensitivity, respectively. The system (2.6)-(2.8) is supplemented with boundary conditions, in the non-dimensional form

$$v(0,t) = 0, \quad v(1,t) = 1\,, \tag{2.10}$$

$$\theta_x(0,t) = 0, \quad \theta_x(1,t) = 0 \tag{2.11}$$

and initial conditions

$$v(x,0) = v_0(x)\,,\ \theta(x,0) = \theta_0(x) > 0,\ \gamma(x,0) = \gamma_0(x) > 0, \tag{2.12}$$

for $x \in [0,1]$. We take $v_{0x} > 0$, in which case a maximum principle shows that $\gamma_t = v_x > 0$ at all times and thus all powers are well defined.

2.1. *Uniform shearing solutions*

System (2.6) admits a special class of solutions describing *uniform shearing*. These are:

$$\begin{aligned} v_s(x,t) &= x, \\ \gamma_s(x,t) &= \gamma_s(t) := t + \gamma_0, \\ \theta_s(x,t) &= \theta_s(t)\,, \end{aligned}$$

where

$$\begin{aligned} \frac{d\theta_s}{dt} &= f(\theta_s, t+\gamma_0, 1), \\ \theta_s(0) &= \theta_0 \end{aligned}$$

and γ_0, θ_0 are positive constants, standing for an initial strain and temperature. The resulting stress is given by the graph of the function

$$\sigma_s(t) = f(\theta_s(t), t+\gamma_0, \dot\gamma_0)\,,$$

which may be interpreted as stress vs. time but also as stress vs. (average) strain. This effective stress-strain curve coincides with the $\sigma_s - t$ graph, and the material exhibits effective hardening in the increasing parts of the graph and effective softening in the decreasing parts. The slope is determined by the sign of the quantity $f_\theta\, f + f_\gamma$. When this sign is negative the combined effect of strain hardening and thermal softening delivers net softening. For a power law (2.8) the uniform shearing solution reads

$$\begin{aligned} \gamma_s(t) &= t + u_0, \\ \theta_s(t) &= \left[\theta_0^{1+\alpha} + \frac{1+\alpha}{m+1}\Big[(t+\gamma_0)^{m+1} - \gamma_0^{m+1}\Big]\right]^{\frac{1}{1+\alpha}}, \\ \sigma_s(t) &= \theta_s^{-\alpha}(t)(t+\gamma_0)^m\,. \end{aligned} \tag{2.13}$$

Observe that, for parameter values ranging in the region $m < \alpha$, $\sigma_s(t)$ may initially increase but eventually decreases with t. We will focus henceforth in this parameter

range, that is in situations that the combined effect of thermal softening and strain hardening results to net softening.

2.2. *A rescaled system*

Motivated by the uniform shearing solutions (2.13), we introduce a rescaling of the variables and of time in the form:

$$\begin{aligned} &\theta(x,t) = (t+1)^{\frac{m+1}{\alpha+1}}\Theta(x,\tau(t)), \quad \gamma(x,t) = (t+1)\Gamma(x,\tau(t)),\\ &\sigma(x,t) = (t+1)^{\frac{m-\alpha}{\alpha+1}}\Sigma(x,\tau(t)), \quad v(x,t) = V(x,\tau(t)), \quad \tau = \ln(1+t). \end{aligned} \tag{2.14}$$

In the new variables the system (2.6)-(2.8) becomes :

$$\begin{aligned} V_\tau &= \frac{1}{r} e^{\frac{m+1}{1+\alpha}\,\tau}\,\Sigma_x\,,\\ \Gamma_\tau &= V_x - \Gamma\,,\\ \Theta_\tau &= \kappa e^{\tau}\Theta_{xx} + \Sigma V_x - \frac{m+1}{1+\alpha}\Theta\,,\\ \Sigma &= \Theta^{-\alpha}\Gamma^m V_x^n\,. \end{aligned} \tag{2.15}$$

The non-dimensional rescaled system (2.15) is the one used to produce the numerical results reported in section 4. Notice that all material related characteristics are integrated in two non-dimensional parameters namely r and κ. For the classical torsional experiment on steels for a sample of size $d = 2.5mm$ with initial velocity $V \in [2.5, 500]$, the initial strain rate $\dot{\gamma}_0$ takes values in the range of 10^3 to $2\cdot 10^5$, $r \in [5\cdot 10^{-5}, 2]$ and the diffusion coefficient $\kappa \in [10^{-5}, 2\cdot 10^{-3}]$.

Although the early deformation can with no considerable error be regarded as adiabatic, when localisation sets and temperature gradients across a band become very large thermal diffusion effects can no longer be regarded as negligible. The morphology of a fully formed band in the late stages of deformation is thus influenced by heat conduction balancing the heat production from plastic work. In Ref. 40, which is probably the only extensive treatment of fully formed shear bands, Walter noticed that, due to heat conduction, the strain rate essentially becomes independent of time in the late stages of deformation, even though the temperature and stress continue to evolve.

3. A finite element method

We consider a finite element discretization of the non-dimensional mathematical model (2.6) coupled with the empirical power law (2.8), augmented with boundary conditions (2.10), (2.11) and initial conditions (2.12). Let $\mathcal{T}_h$ be a partition of $\Omega = [0,1]$, $0 = x_0 < x_1 < \ldots, < x_{M_h} = 1$ consisting of sub-intervals $I = [x_{i-1}, x_i]$ of length $h_i = x_i - x_{i-1}$, $i = 1, \ldots, M_h$ and let $h = \sup_i h_i$. Further let $0 = t_0 < t_1 < \cdots < t_k < \ldots$ be a partition of $[0,\infty)$ with $\delta_k = t_k - t_{k-1}$, $k = 1, 2, \ldots$. We

consider the classical one dimensional C^0 finite element space $\mathcal{S}_{h,p} \subset L^2(\Omega)$, defined on partitions $\mathcal{T}_h$ of Ω

$$\mathcal{S}_h = \mathcal{S}_{h,p} = \left\{ \phi \in C^0(\Omega) : \phi|_I \in \mathbb{P}_p(I), I \in \mathcal{T}_h, \right\}, \quad \dim\mathcal{S}_h = p\, M_h + 1, \tag{3.1}$$

where $\mathbb{P}_p(I)$ denotes the space of polynomials on I of degree at most p.

Remark 3.1. In general we allow the partitions $\mathcal{T}_h$ to have variable size and vary with time, $\mathcal{T}_h = \mathcal{T}_h^k,\ M_h = M_h^k$ and accordingly $\mathcal{S}_h = \mathcal{S}_h^k$. In the sequel, to simplify the notation we drop the dependence on time.

Remark 3.2. Although C^0 finite element spaces are used for interpolating the unknown variables, their spatial derivatives (like v_x) are approximated by completely discontinuous finite elements. This is a different approach from the embedded strong discontinuities method where the discontinuities in the displacement field are embedded explicitly in the finite element spaces and its derivatives are approximated by Dirac masses, Refs. 36, 25, 19, 33, 8, 10.

3.1. *Semidiscrete schemes*

A variational formulation for our model is as follows: we seek functions v_h, θ_h, $\gamma_h, \in \mathcal{S}_h$ such that

$$(v_{h,t}, \phi) = F_h v_{h,x}^n \phi(x)\big|_{x=0}^{x=1} - (F_h v_{h,x}^n, \phi'), \quad \forall \phi \in \mathcal{S}_h, \tag{3.2a}$$

$$(\theta_{h,t}, \psi) = (H_h \theta_h^{-a}, \psi) + \kappa \theta_{h,x} \psi\big|_{x=0}^{x=1} - \kappa(\theta_{h,x}, \psi'), \quad \forall \psi \in \mathcal{S}_h, \tag{3.2b}$$

$$(\gamma_{h,t}, \chi) = (v_{h,x}, \chi), \quad \forall \chi \in \mathcal{S}_h, \tag{3.2c}$$

where

$$F_h \equiv F(\theta_h, \gamma_h) = \frac{1}{r}\, \theta_h^{-a}\, \gamma_h^m \qquad H_h \equiv H(\gamma_h, v_{h,x}) = \gamma_h^m\, v_{h,x}^{n+1}$$

and $(\cdot, \cdot)$ denotes the L^2 inner product. Let $J = \dim\mathcal{S}_h$ we write

$$v_h(x,t) = \sum_{i=1}^{J} V_i(t)\phi_i(x), \quad \theta_h(x,t) = \sum_{i=1}^{J} \theta_i(t)\psi_i(x), \quad \gamma_h(x,t) = \sum_{i=1}^{J} \gamma_i(t)\chi_i(x),$$

$$\text{with} \quad \mathcal{V} = (V_1, \ldots, V_J), \qquad \mathcal{U} = (\theta_1, \ldots, \theta_J) \quad \text{and} \quad \mathcal{G} = (\gamma_1, \ldots, \gamma_J).$$

Using the boundary conditions (2.10) and (2.11), system (3.2a)-(3.2c) can be written in a matrix form

$$\mathcal{M}\dot{\mathcal{V}} = \mathcal{F}(\mathcal{V},\mathcal{U},\mathcal{G}), \qquad \mathcal{V}(t=0) = v_h(x,0) = \mathcal{P}v_0(x), \tag{3.3}$$

$$\mathcal{M}\dot{\mathcal{U}} = \mathcal{H}(\mathcal{V},\mathcal{U},\mathcal{G}), \qquad \mathcal{U}(t=0) = \theta_h(x,t=0) = \mathcal{P}\theta_0(x), \tag{3.4}$$

$$\mathcal{M}\dot{\mathcal{G}} = \mathcal{D}\mathcal{V}, \qquad \mathcal{G}(t=0) = \gamma_h(x,t=0) = \mathcal{P}\gamma_0(x), \tag{3.5}$$

where $\mathcal{M} = (\phi_i, \phi_j),\ \mathcal{D} = (\phi_i', \chi_j),\ i,j = 1, \ldots, J$ are the mass and stiffness-like matrices respectively and

$$\begin{aligned} \mathcal{F}(\mathcal{V},\mathcal{U},\mathcal{G}) &= F_h v_{h,x}^n\big|^{x=1} - (F_h v_{h,x}^n, \phi_j')\ , \\ \mathcal{H}(\mathcal{V},\mathcal{U},\mathcal{G}) &= (H_h \theta_h^{-a}, \psi_j) - \kappa(\theta_{h,x}, \psi_j'),\ j = 1, \ldots, J\ , \end{aligned} \tag{3.6}$$

where $\mathcal{P} : C^0([0,d]) \to \mathcal{S}_h$ denotes either the interpolation or the L^2 projection operator.

3.2. *Fully discrete schemes*

The initial value problem (3.3)-(3.5) is a coupled fully non-linear system of ordinary differential equations and is discretized by a Runge-Kutta method. Let $\mathcal{V}^0 = \mathcal{V}(t = 0)$, $\mathcal{U}^0 = \mathcal{U}(t = 0)$, $\mathcal{G}^0 = \mathcal{G}(t = 0)$, given the solution $\mathcal{V}^k$, $\mathcal{U}^k$, $\mathcal{G}^k$ at time level t_k we compute intermediate values $\mathcal{V}^{k,i}$, $\mathcal{U}^{k,i}$, $\mathcal{G}^{k,i}$ as the solution of the following non-linear system :

$$\begin{aligned}
\mathcal{M}\mathcal{V}^{k,i} &= \mathcal{M}\mathcal{V}^k + \delta_{k+1}\sum_{j=1}^{s} a_{ij}\mathcal{F}(\mathcal{V}^{k,j},\mathcal{U}^{k,j},\mathcal{G}^{k,j}), \quad i = 1,\dots,s,\\
\mathcal{M}\mathcal{U}^{k,i} &= \mathcal{M}\mathcal{U}^k + \delta_{k+1}\sum_{j=1}^{s} a_{ij}\mathcal{H}(\mathcal{V}^{k,j},\mathcal{U}^{k,j},\mathcal{G}^{k,j}), \quad i = 1,\dots,s,\\
\mathcal{M}\mathcal{G}^{k,i} &= \mathcal{M}\mathcal{G}^k + \delta_{k+1}\sum_{j=1}^{s} a_{ij}\mathcal{D}\mathcal{V}^{k,j}, \quad i = 1,\dots,s
\end{aligned} \tag{3.7}$$

and the solution at the next time level t_{k+1} is updated by

$$\begin{aligned}
\mathcal{M}\mathcal{V}^{k+1} &= \mathcal{M}\mathcal{V}^k + \delta_{k+1}\sum_{i=1}^{s} b_i\mathcal{F}(\mathcal{V}^{k,i},\mathcal{U}^{k,i},\mathcal{G}^{k,i}),\\
\mathcal{M}\mathcal{U}^{k+1} &= \mathcal{M}\mathcal{U}^k + \delta_{k+1}\sum_{i=1}^{s} b_i\mathcal{H}(\mathcal{V}^{k,i},\mathcal{U}^{k,i},\mathcal{G}^{k,i}),\\
\mathcal{M}\mathcal{G}^{k+1} &= \mathcal{M}\mathcal{G}^k + \delta_{k+1}\sum_{i=1}^{s} b_i\mathcal{D}\mathcal{V}^{k,i},
\end{aligned} \tag{3.8}$$

where $A = (a_{ij})$, $b = (b_i)$, $i,j = 1,\dots,s$ are the parameters defining an $s-$stage Runge-Kutta method. System (3.7) is a large fully non-linear system and computationally very expensive to solve. Thus we propose an Implicit-Explicit RK (IERK) method to discretize (3.3)-(3.5): in the system (3.7) the unknown variable is treated implicitly while the other variables are treated explicitly. The proposed scheme decouples the system and for each intermediate stage i the equations are solved separately, possibly in parallel:

$$\begin{aligned}
\mathcal{M}\mathcal{V}^{k,i} &= \mathcal{M}\mathcal{V}^k + \delta_{k+1}\sum_{j=1}^{i} a_{ij}\mathcal{F}(\mathcal{V}^{k,j},\mathcal{U}^{k},\mathcal{G}^{k}), \quad i = 1,\dots,s,\\
\mathcal{M}\mathcal{U}^{k,i} &= \mathcal{M}\mathcal{U}^k + \delta_{k+1}\sum_{j=1}^{i} a_{ij}\mathcal{H}(\mathcal{V}^{k},\mathcal{U}^{k,j},\mathcal{G}^{k}), \quad i = 1,\dots,s,\\
\mathcal{M}\mathcal{G}^{k,i} &= \mathcal{M}\mathcal{G}^k + \delta_{k+1}\sum_{j=1}^{i} a_{ij}\mathcal{D}\mathcal{V}^{k,j}, \quad i = 1,\dots,s.
\end{aligned} \tag{3.9}$$

In the simple case where $s = 1,\ A = a_{11} = 1,\ b = b_1 = 1$ (Implicit Euler) the system (3.9),(3.8) is

$$\mathcal{M}\mathcal{V}^{k+1} = \mathcal{M}\mathcal{V}^{k} + \delta_{k+1}\mathcal{F}(\mathcal{V}^{k+1}, \mathcal{U}^{k}, \mathcal{G}^{k}), \tag{3.10a}$$

$$\mathcal{M}\mathcal{U}^{k+1} = \mathcal{M}\mathcal{U}^{k} + \delta_{k+1}\mathcal{H}(\mathcal{V}^{k}, \mathcal{U}^{k+1}, \mathcal{G}^{k}), \tag{3.10b}$$

$$\mathcal{M}\mathcal{G}^{k+1} = \mathcal{M}\mathcal{G}^{k} + \delta_{k+1}\mathcal{D}\mathcal{V}^{k+1}, \tag{3.10c}$$

The last equation (3.10c) is linear while (3.10a) and (3.10b) are non-linear. The non-linear equations are linearized using Newton's method. In particular each of these equations is of the form :

$$\begin{aligned} &\text{solve } \mathcal{A}(\mathcal{X}, \mathcal{Y}, \mathcal{Z}) = 0, \quad \text{for } \mathcal{X} \text{ where ,} \\ &\qquad \mathcal{A}(\mathcal{X}, \mathcal{Y}, \mathcal{Z}) = \mathcal{M}\bar{\mathcal{X}} + \delta\mathcal{B}(\mathcal{X}, \mathcal{Y}, \mathcal{Z}) - \mathcal{M}\mathcal{X} \quad \text{and } \bar{\mathcal{X}}, \mathcal{Y}, \mathcal{Z} \text{ are given.} \end{aligned} \tag{3.11}$$

Newton's method for (3.11) is

$$D\mathcal{A}(\mathcal{W}_\ell)(\mathcal{W}_{\ell+1} - \mathcal{W}_\ell) = -\mathcal{A}(\mathcal{W}_\ell), \quad \mathcal{W} = (\mathcal{X}, \mathcal{Y}, \mathcal{Z}), \quad \ell = 0, \ldots, \ell_k, \tag{3.12}$$

where $D\mathcal{A}$ denotes the Frechet derivative of $\mathcal{A}$. The starting values for the Newton's iteration are taken to be : $\mathcal{V}_0^{k+1} = \mathcal{V}^k$, $\mathcal{U}_0^{k+1} = \mathcal{U}^k$ and we set $\mathcal{V}^{k+1} = \mathcal{V}_{\ell_k}^{k+1}$, $\mathcal{U}^{k+1} = \mathcal{U}_{\ell_k}^{k+1}$. In practice $\ell_k = 2$ or 3 is enough to guarantee convergence of the iterative procedure. The discretization of system (2.15) is done in a completely analogous fashion.

3.3. *Adaptive refinement strategy*

The width of the shearing band is of the order of at most a few micrometers (orders of magnitude less than the overall size of the material surrounding the band), whereas the lateral extent may be several millimetres in length. As the morphology of a shear band exhibits such a fine transverse scale, it would be costly to resolve the bands fully in a large-scale computation. A resolution of the order of $10\mu m$ or less would be required for many materials in order to follow the deformation across the band in detail. When a fixed mesh is used and the tip of a peak of a state variable becomes narrower than the mesh spacing then it will be the length scale of the grid that regularises the calculation rather than the physical and constitutive features of the material. Thus, there is a strong dependence between the peaks of the state variables and the mesh size h (fixed mesh). We believe that the adaptive computation is much more accurate than any of the computations on a fixed mesh. Capturing numerically this singular behaviour is not a trivial task. Special adaptive techniques in space as well in time have to be used to capture correctly the underlying phenomenon. We describe now the adaptive mechanisms that are used.

3.3.1. *Spatial mesh refinement.*

The adaptive mesh refinement strategy presented here is motivated by the work in Ref. 9, Ref. 1 and Ref. 34 where a similar strategy is used for the numerical

simulation of blow-up solutions of the generalised KdV and non-linear focusing Schrödinger equations respectively. The proposed method is able to capture the growth of the solution using only, at the final mesh, about 40% extra spatial grid points to the initial discretization.

In the unstable regime $q = -\alpha+m+n < 0$, as time increases, $v_x,\ \theta,\ \gamma$ grow near a point $x^\star \in \Omega$. The proposed spatial adaptive mechanism acts in two ways : first locates the singular point $x^\star$ automatically and secondly increases locally the resolution of the finite element scheme by refining the mesh in a small neighbourhood around $x^\star$. The adaptive mesh refinement strategy is motivated by a local $L^\infty - L^1$ inverse inequality that elements of $\mathcal{S}_h$ satisfy on $I \in \mathcal{T}_h$, Ref. 14. We assume that the partition $\mathcal{T}_h$ satisfies (*inverse assumption*): $\exists c_0 > 0 \in \mathbb{R}$ such that $h \leq c_0 \min_i h_i$. Then for $\chi \in \mathcal{S}_h$ we have

$$\|\chi\|_{L^\infty(I)} < C h_i^{-1} \|\chi\|_{L^1(I)}, \qquad \text{with } \ C := C(\Omega, p, c_0). \tag{3.13}$$

For $\chi = v^k_{h,x}$, (3.13) shows that the growth of the L^∞ norm of $v_{h,x}$ is bounded by the size of h_i and the L^1 norm of $v_{h,x}$ on I, which does not change, (2.10). Thus at time level k an interval I of the partition $\mathcal{T}_h$ is refined, its spatial size h_i is halved, if the following criterion is satisfied

$$\|v^k_{h,x}\|_{L^\infty(I)} h_i > \epsilon_h \|v^k_{h,x}\|_{L^1(I)}, \tag{3.14}$$

where $\epsilon_h \sim 1$. The interval I satisfying (3.14) contains $x^\star$ and we allow $v_{h,x}$ to grow by refining the mesh, in one or at most two intervals, around $x^\star$. Using this technique, mesh sizes of the order of 10^{-13} of the size of the specimen, are used to resolve the singularity, Fig. 2. On the other hand due to the local nature of the adaptive technique, very few elements are affected, thus the new finite element spaces and related stiffness matrices, can be computed with small extra computational effort. Finally, any function on the old mesh is embedded in the new one by linear interpolation.

3.3.2. *Time adaptivity*

In time the solution grows rapidly near the singularity point $x^\star$, thus controlling the size of the time step δ_k is necessary. Choosing δ_k adaptively is a very delicate issue in these type of simulations. Our time step selection strategy is motivated by preserving a physical property of the system, in particular the energy $E(t)$:

$$E(t) := \int_0^1 \left[\frac{\beta r}{2} v^2(x,t) + \theta(x,t) \right] dx. \tag{3.15}$$

Using (2.6) and the boundary conditions we get

$$\frac{\partial E}{\partial t} = \sigma|_{x=1}. \tag{3.16}$$

Thus to preserve the energy in time up to first order we define the time step size δ_{k+1} as

$$\delta_{k+1} = \min\{\epsilon_\delta \frac{|E_h^{n+1} - E_h^n|}{\sigma_h^{k+1}|_{x=1}}, \delta_0\} \tag{3.17}$$

where $E_h^n = \int_0^d \left[\frac{r}{2} v_h^2(x, t^n) + \theta_h(x, t^n)\right] dx$, δ_0 a given time step threshold and $\epsilon_\delta \sim 1$.

4. Numerical Experiments

In the sequel, we present the results of several numerical experiments that illustrate the various features and properties of the model (2.6). All the experiments were performed on a Pentium 4 workstation running Linux at 2.4GHz, using a code that implements in double precision the fully discrete schemes for the equivalent rescaled system (2.15). Working with (2.15) has the advantage that we can easily access long times, due to the relation $\tau = \ln(1+t)$ between the original time t and the rescaled time τ. In all numerical runs, unless otherwise mentioned, linear finite element are used for the spatial discretization and the implicit Euler method (3.10) for time stepping.

4.1. *Numerical results*

We present a series of numerical results illustrating the features of system (2.6). The numerical results presented here are obtained by discretizing (2.15). The material parameters $\alpha,\ m, n$ are selected in two representative regions:

- Region I (Stable case) : $-\alpha + m + n > 0$,
- Region II (Shear Band) : $-\alpha + m + n < 0$.

Initial conditions. There are different choices of initial conditions throughout the literature for (2.6), the majority of them are perturbations of the uniform shearing solution (2.13). One type consists of introducing, at the centre of the slab, a small initial temperature perturbation of Gaussian form, added to the homogeneous initial temperature θ_I, as used elsewhere in the literature, see Refs. 40, 4. Another type of initial perturbation consists of introducing a small perturbation to the uniform

shearing solutions in all three variables v, θ, γ:

$$v_0(x) = \begin{cases} \tan(\frac{\pi}{q})x & 0 \le x \le \frac{1}{2} - g \\ \frac{1}{2}(1 - \tan(\frac{\pi}{q}))\left[1 - \cos(\frac{\pi(x-\frac{1}{2}+g)}{2g}\right] + x\tan(\frac{\pi}{q}) & \frac{1}{2} - g < x < \frac{1}{2} + g \\ 1 - \tan(\frac{\pi}{q})(1-x) & \frac{1}{2} + g \le x \le 1 \end{cases}$$

$$\theta_0(x) = \begin{cases} 1.01 + 0.01\cos(\frac{\pi(x-\frac{1}{2})}{g}) & \frac{1}{2} - g < x < \frac{1}{2} + g \\ 1 & \text{otherwise} \end{cases}$$

$$\gamma_0(x) = \begin{cases} 0.011 + 10^{-3}\cos(\frac{\pi(x-\frac{1}{2})}{g}) & \frac{1}{2} - g < x < \frac{1}{2} + g \\ 0.01 & \text{otherwise} \end{cases} \qquad \text{(ICA)}$$

where $g = 0.02$, $q = 4.0001$.A third commonly used perturbation is that of a geometric imperfection, like the symmetric groove in the centre of the slab. All these choices, in the unstable case (Region II), will give rise to a single shear band at the centre of the slab. In all the experiments reported here we use initial conditions of the type (ICA).

Remark 4.1. The equations that are numerically resolved are in non-dimensional form. The parameters α, m, n are selected in either of the regions (I) or (II), and we systematically study certain aspects of the dependence in the dimensionless numbers r and κ. In the Figures below "TIME" stands for the physical non-dimensional time $\hat{t}$ (2.5), while τ is defined in (2.14).

4.1.1. *The stable case (Region I).*

First we consider adiabatic deformation $\kappa = 0$ with parameters in the stable region : $q = -\alpha + n + m > 0$. We compute the solution of (2.15) for $\alpha = 0.5,\ n = 0.75,\ m = 0.25$. The solution variables can be seen in Figure 1 at different time instances. The computed solution approaches very fast the uniform shearing solution (2.13).

4.1.2. *Adiabatic Shear Band (Region II).*

We consider next adiabatic deformations ($\kappa = 0$) with parameters taking values in the unstable region : $-\alpha + n + m < 0$ where we expect formation of shear bands; specifically, we take $\alpha = 2,\ m = 0.25,\ n = 0.2$. To be able to capture the singular behaviour of the solution the use of the adaptive techniques (3.14), (3.17) is mandatory. A typical behaviour of the adaptive spatial and time refinement method is shown in Figure 2. In particular, Figure 2(left) shows the evolution in time of the smallest spatial length $h_{\min}$ and the time step δ_k produced by the adaptive strategy. The proposed spatial adaptive process (3.14) reduces the mesh size appropriately, reaching a value of $h_{\min} \sim 10^{-13}$, to capture the immense growth of the solution (v_x, θ, γ) at the shear band point. Furthermore using (3.17), the time step δ_k is refined appropriately to follow the rapidly changing solution with $\delta_k \sim 10^{-9}$ at final time. On the other hand, Figure 2(right) shows the distribution of h_i's over

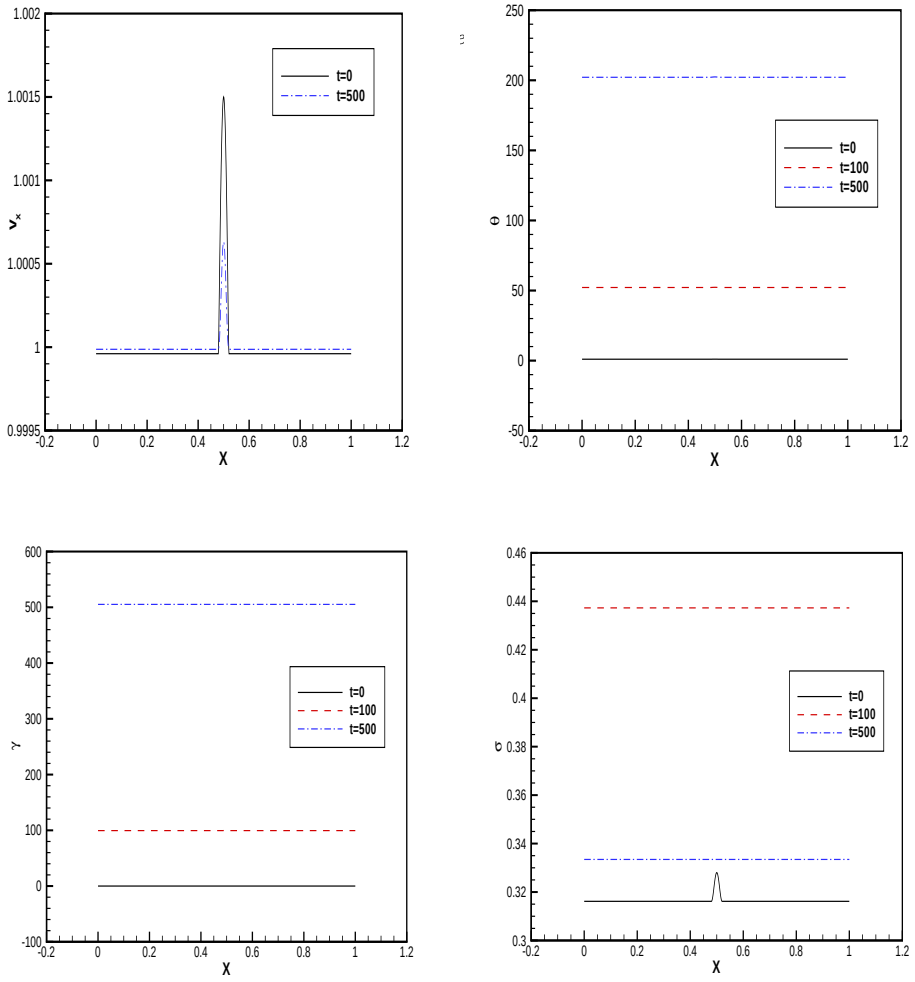

Fig. 1. Region I : solution at $t = 0$, $t = 100$ and $t = 500$

the unit slab at final time of the simulation. We notice that the mesh refinement technique (3.14) locates the singular point correctly and reduces the mesh size where necessary.

We compute the solution of system (2.15) with $\alpha = 2$, $m = 0.25$, $n = 0.2$. The choice of initial condition (ICA) will yield a shear band located at $x = \frac{1}{2}$. The computed solution of the system, up to time $t \sim 2.62$, is shown in Figures 3, 4, 5, 6 and 7. The singular behaviour of the solution is fully resolved using the adaptive techniques (3.14), (3.17) with $\epsilon_h = 1.0025$ and $\delta_0 = 10^{-5}$. In Figure 8, we show the evolution in time of the v_x, θ, γ, σ at the shear band point $x = \frac{1}{2}$. The strain rate $v_x(\gamma_t)$ has reached a value of about 10^8, the temperature has risen about 3000 times the initial one, the strain has grown about 6 orders in magnitude and the stress almost collapsed and reached a value of 0.00056. As can be seen from Figure 6, (bottom right) the stress reaches a very small value thus the diffusion process

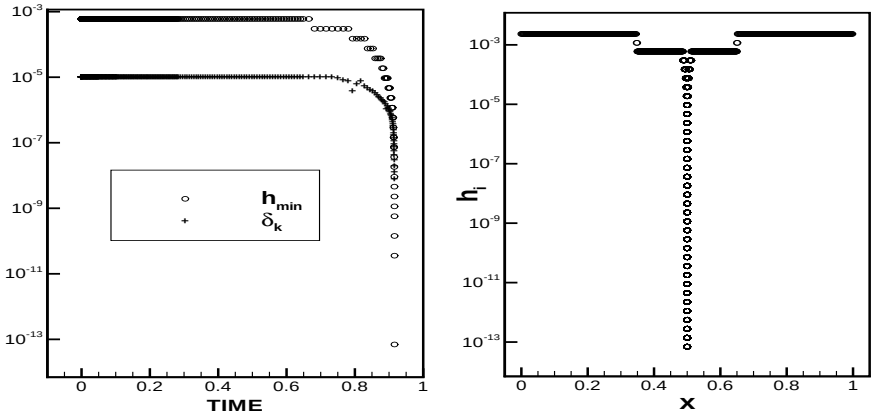

Fig. 2. Adaptivity: evolution of $h_{\min}, \delta_k$(left), final distribution of h_i(right)

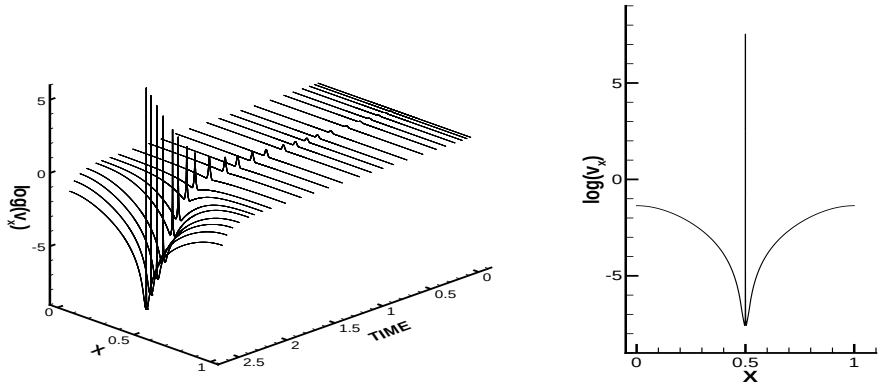

Fig. 3. Region II : Strain rate $v_x(\gamma_t)$ in log-scale: evolution (left), final time (right)

collapses and no information gets across the shear band. Further the oscillations are not a numerical artifact and are caused by the very nature of the underlying instability which is of a backward parabolic type, see Ref. 28.

We also study the effect of the non-dimensional parameter r on the solution of system (2.15). As already mentioned in the classical torsional experiment on a steel sample of size $d = 2.5mm$, Ref. 15, for typical values of initial velocity V, the parameter r takes values in the interval $[5 \cdot 10^{-5}, 2]$. Our results, away from the shear band point, are in excellent agreement with those presented in Ref. 15, while at the shear band point our results exhibit better resolution than in Ref. 15.

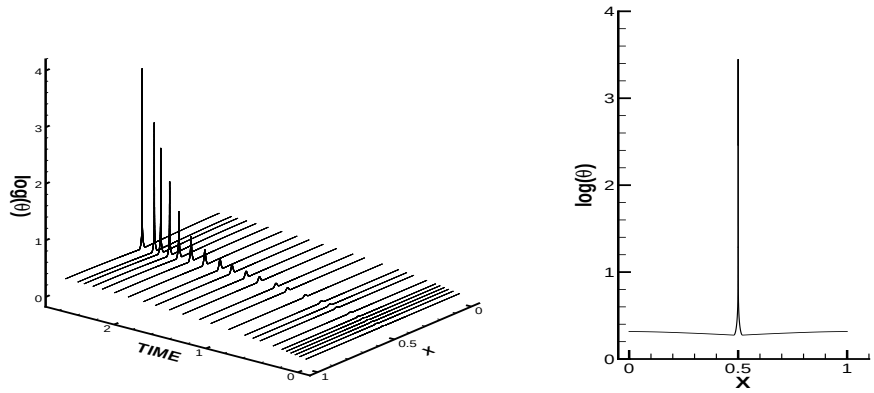

Fig. 4. Region II : Temperature θ in log-scale: evolution (left), final time (right)

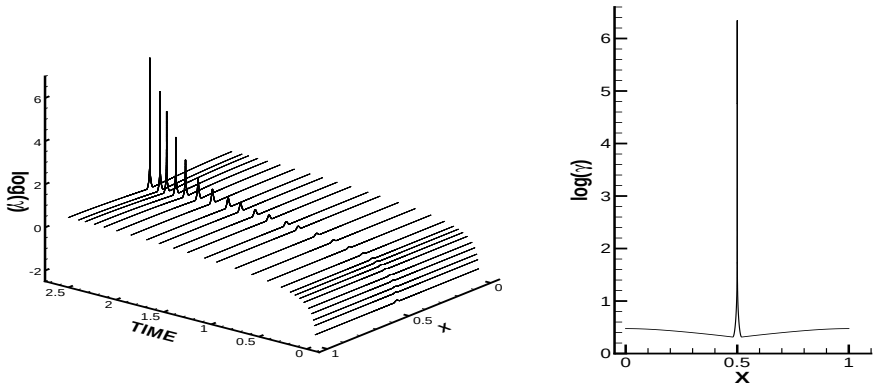

Fig. 5. Region II : Strain γ in log-scale: evolution (left), final time (right)

In Figure 9, for different values of the parameter r, we compare the evolution in time of the stress values at the shear band point. Notice that the initiation time of localisation is almost identical for all values of the parameter r. On the other hand as the value of r decreases the localisation is more abrupt thus diminishing the time when the localisation takes place. This type of behaviour is observed also for v_x, θ and γ.

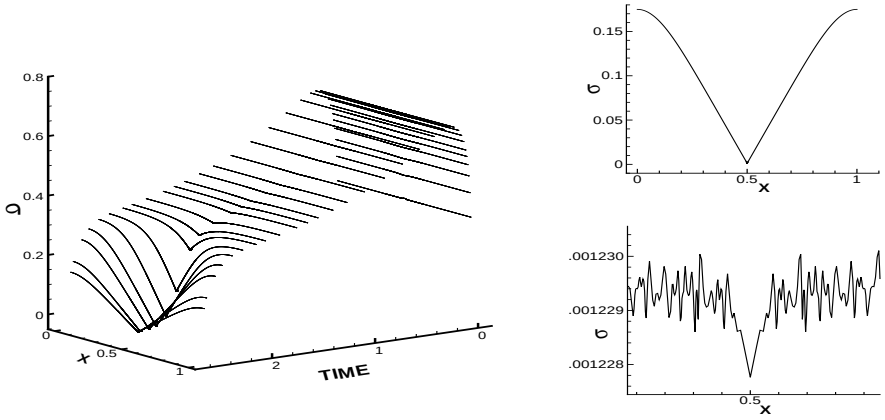

Fig. 6. Region II : Stress σ: evolution (left), final time (top right), zoom (bottom right)

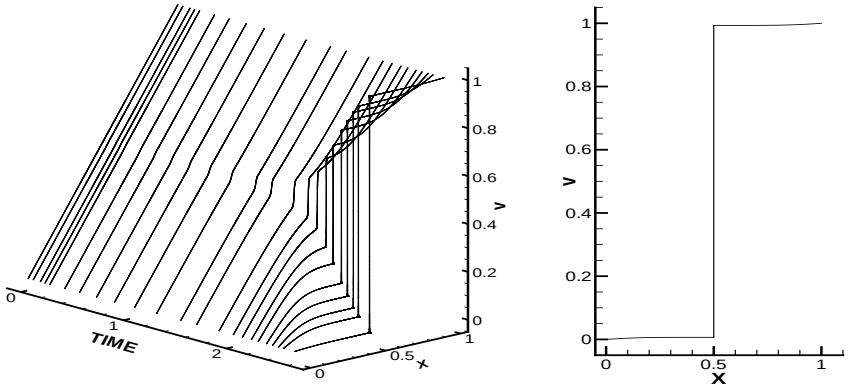

Fig. 7. Region II : Velocity v: evolution (left), final time (right)

4.2. *Effect of heat diffusion*

Next, we compute the solution of system (2.15) in the non-adiabatic case $\kappa > 0$. The heat diffusion coefficient is taken $\kappa = 10^{-6}$ while the thermomechanical parameters α, m and n are as in the previous runs in the unstable case Region II. The evolution of the state variables is presented in Figures 10, 11, 12, 13, 14. The behaviour depicted by the numerical simulations holds true for other values of the heat diffusion coefficient that we tested but do not present here. Namely, after a transient period of localisation, the inhomogeneities of the state variables eventually dissipate and the underlying *uniform shearing solution* (2.13) emerges.

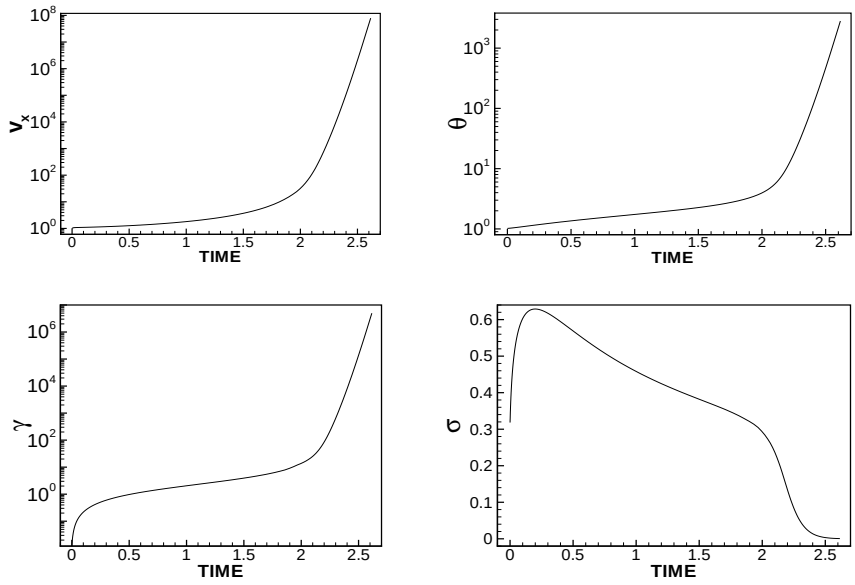

Fig. 8. Region II : Evolution of $v_x,\ \theta,\ \gamma,\ \sigma$ at $x = \frac{1}{2}$. v_x and γ are in log-scale.

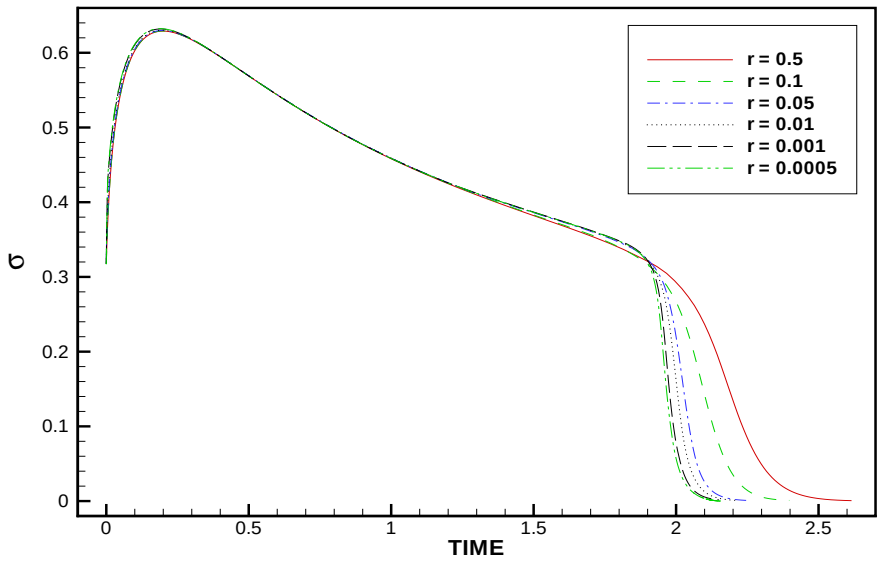

Fig. 9. Evolution of σ at $x = \frac{1}{2}$ for various values of r

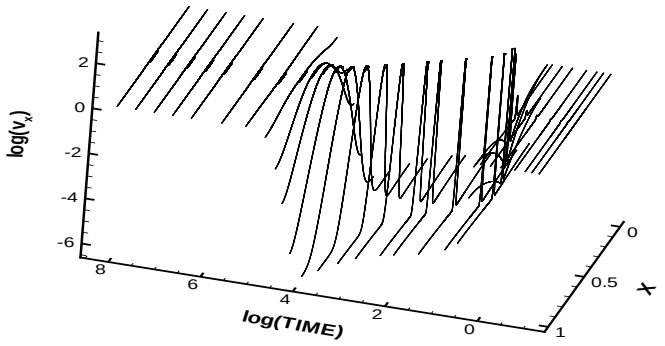

Fig. 10. Non-adiabatic case : $\kappa = 10^{-6}$, Strain rate $v_x, (\gamma_t)$ in log-scale: evolution (left), final time (right)

.

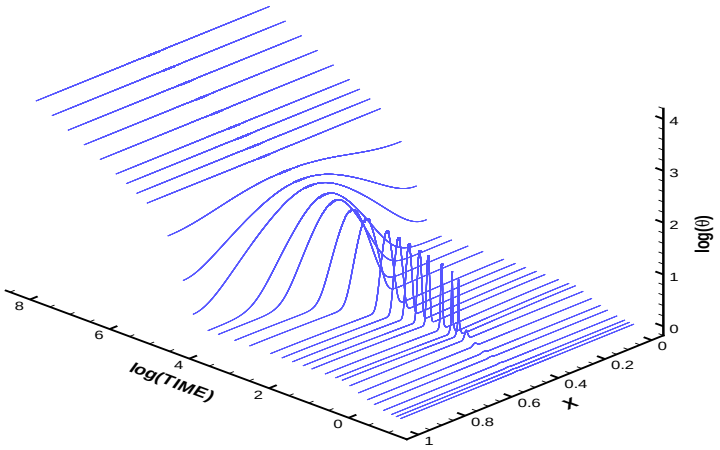

Fig. 11. Non-adiabatic case : $\kappa = 10^{-6}$, Evolution of temperature θ in log-scale

The effect of the value of the heat diffusion coefficient is restricted in the localisation stage as one may observe in the Figures 15, 16, 17, 18. The smaller the heat diffusion coefficient is, the stronger the rate of localisation. The effect of the heat diffusion on the initiation of the localisation process is negligible, and thus the early stages of deformation that can be regarded as adiabatic. By contrast, heat diffusion has an effect on the subsequent evolution and development period of the band. Finally, heat diffusion not only delays but even stops the development of the band and returns the solution to uniform shear, but the latter process takes a very

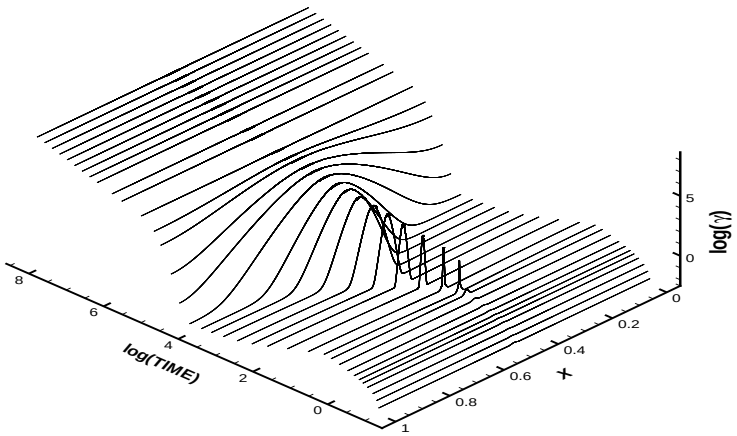

Fig. 12. Non-adiabatic case : $\kappa = 10^{-6}$, Evolution of strain γ in log-scale

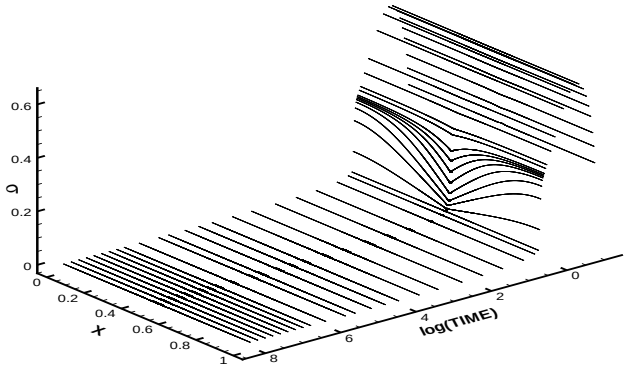

Fig. 13. Non-adiabatic case : $\kappa = 10^{-6}$, Evolution of stress σ

long time and might not be observable in practice.

5. Discussion

Adaptive finite elements computations are employed to tackle the multiscale response of rate-dependent materials subjected to simple shearing deformations. Numerical solutions are a necessity in order to fully describe the singular phenomenon associated with localisation. The adaptive mesh refinement strategy, as well as the time step control are discussed and the accuracy of the resulting schemes is tested with the expected numerical order of accuracy observed in all cases. The consti-

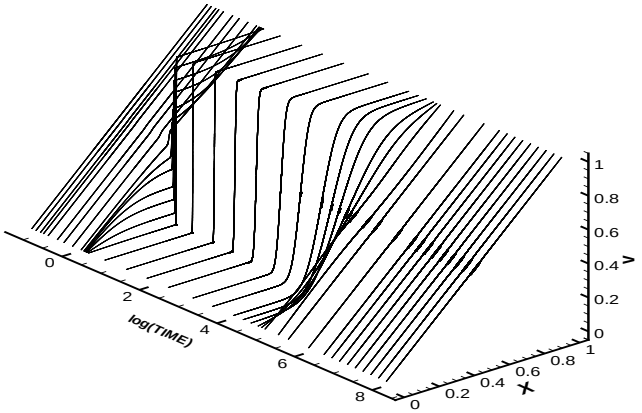

Fig. 14. Non-adiabatic case : $\kappa = 10^{-6}$, Evolution of velocity v

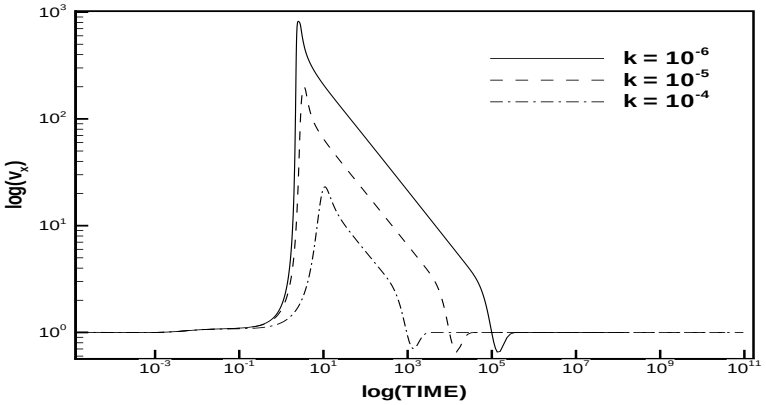

Fig. 15. Non-adiabatic case : different heat diffusion coefficients κ, Strain rate γ_t in log-scale at the centre of the slab.

tutive law used is of the power law type that has been used extensively in the literature and allows considerable flexibility in fitting experimental data over an extended range. The numerical runs indicate unstable response for thermomechanical parameters taking values in the region $-\alpha + n + m < 0$. The early stages of deformation can be regarded as adiabatic, because high strain rates do make heat conduction unimportant at that stage. At this stage, shear band formation occurs with a simultaneous collapse of diffusion across the band.

Once localisation sets in, heat conduction plays an important role in the subsequent evolution. Actually there exists a critical time t_{cr} above which the local rate

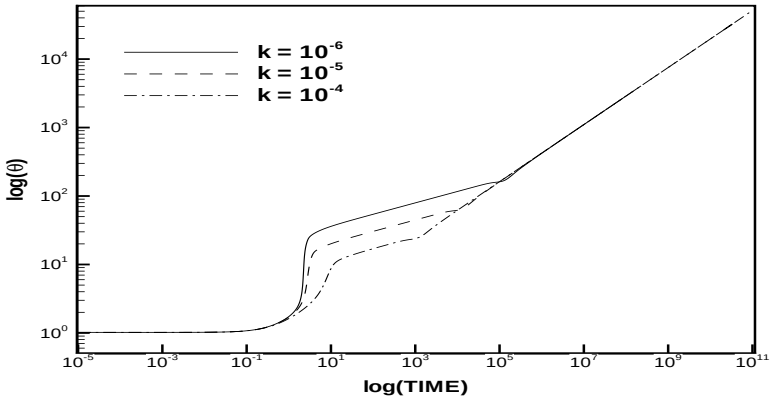

Fig. 16. Non-adiabatic case : different heat diffusion coefficients κ, Temperature θ in log-scale at the centre of the slab.

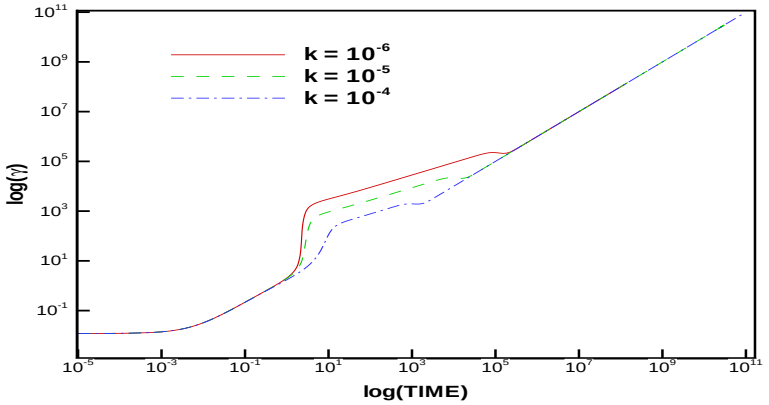

Fig. 17. Non-adiabatic case : for different heat diffusion coefficients κ, Strain γ in log-scale at the centre of the slab.

of heat generation is less than the rate of heat diffusion from the band to the outside colder material. Beyond this critical time the inhomogeneities in the solutions are dissipated and the outcome (assuming that the material has not already fractured, or changed phase) would be for the deformation to dissipate and approach an underlying *uniform shearing solution*. The value of thermal diffusivity κ affects materially the localisation rate and the critical time t_{cr} defined above, while its effect on the initiation time for shear band formation is negligible. Namely, the smaller the value of thermal diffusivity, the stronger the localisation rate and the longer the critical

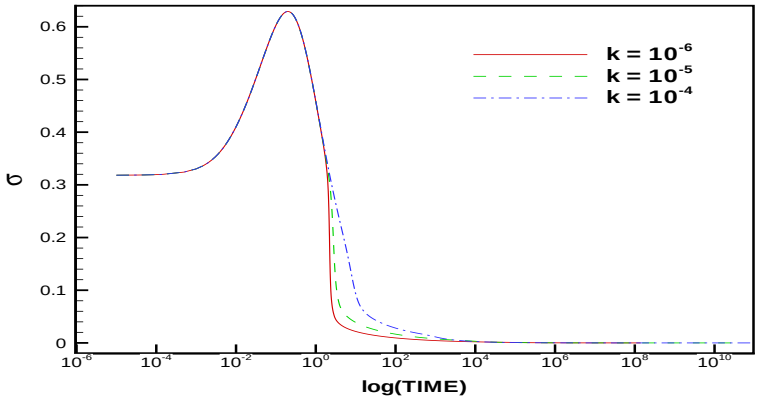

Fig. 18. Non-adiabatic case : different heat diffusion coefficients κ, Stress σ at the centre of the slab.

time.

Acknowledgements

Partially supported by the National Science Foundation, and by the program "Pythagoras" of the Greek Secretariat of Research. The authors would like to thank the anonymous referee's for their valuable comments and suggestions.

References

1. Akrivis G.D, Dougalis V.A, Karakashian O.A, McKinney W.R, *Numerical approximation of blow-up of radially symmetric solutions of the non-linear Schrödinger equation*, SIAM J. Sci. Computing, vol. 25, no. 1, pp. 186-212, 2003
2. Batra R.C. and Gummalla R.R., *Effect of material and geometric parameters on deformations near the notch-tip of a dynamically loaded prenotched plate*, International Journal of Fracture, 101, pp. 99-140, 2000.
3. Batra R.C. and Ravinsankar M.V.S.,*Three-dimensional simulation of the Kalthoff experiment*, International Journal of Fracture, 105, pp. 161-186, 2000
4. Batra, R.C. and Ko, K.I., *An adaptive refinement technique for the analysis of shear bands in plain strain compression of a thermoplastic solid*, Appl. Mech. Rev. 45, 123, 1992.
5. Batra, R.C. and Kim, C.H., *An adaptive mesh refinement technique for the analysis of adiabatic shear banding*, Mechanics Research Communications, 17(2), pp. 81-91, 1990
6. Batra, R.C. and Hwang, J., *An adaptive mesh refinement technique for two-dimensional shear band problems*, Computational Mechanics, 12(4), pp. 255-268, 1993
7. Baxevanis,Th. and Charalambakis, N., *The role of material non-homogeneities*

on the formation and evolution of strain non-uniformities in thermoviscoplastic shearing, Quarterly of Applied Mathematics, 62 (1) pp. 97-116, 2004

8. Belytschko T., Fish J. and Engelmann BE, *A finite element with embedded localization zones*, Computer Methods in Applied Mechanics and Engineering, 70, pp. 5989, 1988.
9. Bona J.L, Dougalis V.A, Karakashian O.A, McKinney W.R, *Fully discrete methods with grid refinement for the generalised Korteweg-de-Vries equation*, Viscous Profile and Numerical Methods for shock waves, M. Shearer ed., SIAM, pp. 1-11, 1991
10. Borst, R. *Some recent issues in computational failure mechanics*, Int. J. Numer. Meth. Engng. 52, pp. 6395, 2001.
11. Burns T. J. and Davies M.A., *On repeated adiabatic shear band formation during high speed machining*, International Journal of Plasticity, 18 (4), pp. 507-530, 2002.
12. Charalambakis, N and Murat, F., *Approximation by finite elements, existence and uniqueness for a model of stratified thermoviscoplastic materials*, Ricerche di Matematica, 55, pp. 171218, 2006
13. Chen, L. and Batra R.C., *The asymptotic structure of a shear band in mode-II deformations*, International Journal of Engineering Science, 37, pp. 895-919, 1999.
14. Ciarlet, P.G, *The finite element method for elliptic problems*, North Holland, 1978.
15. Clifton, R.J., Duffy, J., Hartley, K.A. and Shawki, T.G., *On critical conditions for shear band formation at high strain-rates*, Scripta Met. 18, pp. 443-448, 1984.
16. Clifton R.J., *High strain rate behaviour of metals*, Appl. Mech. Revs. 43(5), S9,1990
17. Dafermos, C.M. and Hsiao,L., *Adiabatic shearing of incompressible fluids with temperature dependent viscosity*, Quart. Appl. Math 41, 45-58, 1983.
18. Drew, D.A. and Flaherty, J.E., *Adaptive finite element methods and the numerical solution of shear band problems*, in Phase Transformations and Material Instabilities in Solids (Madison, WI.1983), Publ. Math. Res. Center Univ.-Wisconsin (Academic Press, Orlando, FL, 1984), Vol. 52, p.37,1984.
19. Dvorkin, E.N, Cuitin, A.M and Gioia, G. *Finite elements with displacement interpolated embedded localization lines insensitive to mesh size and distortions*, Int. J. Numer. Methods Engrg. 30, pp. 541564, 1990.
20. Estep, D.J., Lunel, S.M.V. and Williams, R.D., *Analysis of shear layers in a fluid with temperature-dependent Viscosity*, Comp. Phys. 173, 17-60, 2001.
21. French, D.A., *Computation of large shear deformations of a thermoplastic material*, Numer. Meth. Part. Differential Equations 12, 393, 1996
22. French, D.A. and Garcia, S.M.F., *Finite element approximation of an evolution problem modelling shear band formation* Comp. Meth. Appl. Mech. Eng. 118, 153, 1994.
23. Gilat A. and Cheng C.S., *Modelling torsional split Hopkinson bar tests at strain rates above 10.000 s-1*, International Journal of Plasticity, 18 (5-6), 787-799, 2002.
24. Garaizar, F.X and Trangenstein, J., *Adaptive mesh refinement and front-tracking for shear bands in a antiplane shear model*, SIAM J. Scientific Computing, 20 (2), pp. 750-779, 1998.
25. Hansbo, A. and Hansbo, P, *A finite element method for the simulation of strong and weak discontinuities in solid mechanics*, Comput. Methods Appl. Mech.

Engrg. 193, pp. 35233540, 2004
26. Hartley K.A., Duffy J., Hawley R.J., *Measurement of the temperature profile during shear band formation in steels deforming at high strain-rates*, J. Mech. Phys. Solids 35, 283-301, 1987.
27. Kalthoff J.F., *Modes in dynamic shear failure in solids*, International Journal of Fracture, 101, 1-31, 2000.
28. Katsaounis Th. and Tzavaras A.E., *Effective equations for localisation and shear band formation*, SIAM J. of Applied Mathematics, 69, no. 6, pp. 1618-1643, 2009.
29. Marchand A. and Duffy J., *An experimental study of the formation process of adiabatic shear bands in a structural steel*, J. Mech. Phys. Solids, 36 (3), 251-283, 1988.
30. Molinari A. and Clifton R.J., *Localisation de la deformation viscoplastique en cisaillement simple, Resultats exacts en theorie non-lineaire*, Comptes Rendus Academie des Sciences, II, 296, 1-4, 1983.
31. Molinari, A. and Clifton, R.J., *Analytical characterisation of shear localisation in thermoviscoplastic materials*, Journal of Applied Mechanics 54, 806-812, 1987.
32. J.H. Maddocks and R. Malek-Madani, *Steady-state shear-bands in thermoplasticity. I. Vanishing yield stress*, Internat. J. Solids Structures, 29, pp. 2039–2061, 1992.
33. Mosler, J. *Modeling strong discontinuities at finite strainsA novel numerical implementation*, Comput. Methods Appl. Mech. Engrg. 195, pp. 43964419, 2006.
34. Plexousakis M, *An adaptive non-conforming finite element method for the nonlinear Schrodinger equation*, PhD. Thesis, Univ. of Tennessee, 1996
35. Rogers H.C., *Adiabatic plastic deformation*, Ann. Rev. Mat. Sci. 9, 283-311, 1979.
36. Simo J.C., Oliver J. and Armero, F, *An analysis of strong discontinuities induced by strain-softening in rate-independent inelastic solids*, Computational Mechanics, 12, pp. 277-296, 1993.
37. Tzavaras, A.E., *Plastic shearing of materials exhibiting strain hardening or strain softening*, Arch. Rat. Mech. Anal. 94, 39-58, 1986.
38. Tzavaras, A.E., *Effect of thermal softening in shearing of strain-rate dependent materials*, Arch. Rat. Mech. Anal. 99, 349-374, 1987.
39. Tzavaras, A.E., *Non-linear analysis techniques for shear band formation at high strain rates*, Appl. Mech. Reviews 45, 82-94, 1992.
40. Walter J.W., *Numerical experiments on adiabatic shear band formation in one dimension.* International Journal of Plasticity, 8, 657-693, 1992.
41. Wright T.W., *The Physics and Mathematics of Shear Bands*, Cambridge University Press, 2002.
42. Wright, T.W. and Walter, J.W., *On stress collapse in adiabatic shear bands*, J. Mech. Phys. Solids 35, 701-720, 1987.
43. Wright T.W. and Walter J.W., *The asymptotic structure of an adiabatic shear band in antiplane motion*, Journal of the Mechanics and Physics of Solids, 44, 77-97, 1996.